NUMERICAL INVESTIGATION OF GRAVITATIONAL TURBULENT MIXING WITH ALTERNATING ACCELERATION

O.Sin'kova, V.Sofronov, V.Statsenko, Yu.Yanilkin, V.Zhmaylo.

Paper to be presented at International Workshop on Physics of Compressible Turbulent Mixing (Cambridge, July 2004)

Direct numerical simulation by gas dynamic 3D TREK code is used to investigate the development of turbulence in gravity field at a plane interface of two incompressible fluids (gases) with density difference n=3. The paper considers a case, when acceleration changes sign at a certain time. Computation results are compared to the corresponding available data of experiments.

The problem of turbulent mixing under constant gravity force (constant acceleration) creating unstable conditions at a plane interface between two incompressible fluids (gases) has been investigated both experimentally (Refs.[1-4]) and numerically (Refs.[2,5-8]) using direct 3D simulation method.

Refs.[9,10] describe the experiments carried out with changes of acceleration sign that cause stable conditions at the interface. The corresponding problem was solved investigated numerically in Ref.[11] using the phenomenological turbulence model of the type described in Ref.[12]; in Ref.[13] described was carried out direct 3D numerical simulation, however, none of them observed the effect of the reduced mixing zone during the stability phase.

This paper describes computational investigation of the turbulent mixing problem at a plane interface between two incompressible fluids with density difference n=3 and alternating acceleration using DNS by 3D code TREK.

In one variant of computations materials are considered to be different, i.e. they have different densities, energies and volume fractions (concentrations). Such approach leads to a significant agreement with the results of measurements. A detailed enough grid 200x200x400 is used.

Note that the similar problem was simulated in one-fluid approximation (gases were described as one material) during 3D computations described in Ref.[6]. This work shows no decrease (separation) of the mixing zone after the acceleration sign has change. The assumption was that absence of separation was due to the use of the one-fluid approach leading to computational homogeneous mixing of materials in view of a large scheme viscosity. The two-fluid approach is free of such a disadvantage at interfaces and mixing, in such a case, is heterogeneous, similar to the experiments described in Refs,[9,10].

To achieve clear understanding of this issue, the problem above is also investigated here using the one-fluid approach, both by 3D gas dynamic (GD) code and hydrodynamic (HD) code (providing the flow incompressibility) of TREK complex. These computations were carried out using a computational grid 100x100x200; for comparison, we also used such grid for computations with two concentrations.

Numerical arrays of hydrodynamic quantities from 3D computations are used to find moments of these quantities (diagonal components of Reynolds tensor (turbulent energy), turbulent flows, profiles of density and its mean-square fluctuations), as well as the single-point function of concentration probability density.

This problem was also investigated numerically using phenomenological $k-\varepsilon$ model of turbulence.

1. Setting up computations by TREK code

With the use of gas dynamic code, the problem is formulated similar to that in Refs.[6-8]: at initial time two half-spaces separated by plane z= z_c =0 are filled with rest ideal gases of densities ρ_1=1 and ρ_2=n (n=3, Atwood number A=0.5). The initial geometry of the problem is shown in Fig.1.

Gravitational acceleration at $t \le t^*$=3 is $g_z \equiv -g = -1$ and directed from the heavy substance towards the light one. At $t > t^*$, $g_z \equiv g_{12}$ = 22/75, this agrees with the experiment.

At initial time, random perturbations of density are generated at the interface (a layer 1 cell thick): δρ= ± $\rho_1 \cdot \delta$, where δ= 0.1. Gas dynamics equations are solved for an ideal two-material medium (with zero molecular viscosity and thermal conductivity).

The computational domain is a parallelepiped with a vertical side Λ=2. The parallelepiped's horizontal face is a square with side $L_x = L_y$ =1.

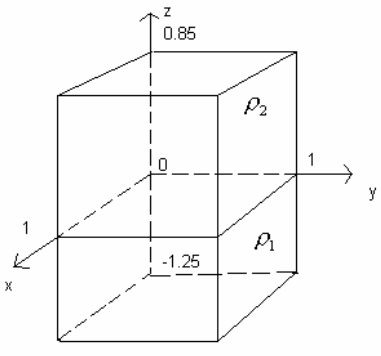

Fig.1. The initial geometry

The initial pressure profile is specified basing on the requirement of hydrostatic equilibrium:

$$p(z) = p_0 - \int_{z_2}^{z} \rho(z) \cdot g \cdot dz \ , \ p_0 = 20.$$

Here, the upper face coordinate is z_2 = 0.85, the lower face coordinate is z_1 = -1.15,

In computation with grid N_x=200, p_0=8.7 and for grid N_x=100 p_0=23.7. Thus, p_0 is increased for the coarse grid in order to reduce computational oscillations during a stable phase.

The value of pressure p_0 is such as to provide good satisfaction of the incompressibility requirement for the given turbulent flow: $k=\xi L_t g \ll \gamma p/\rho$, where ξ=const<<1, $L_t<\Lambda$, L_t is TMZ width, k is turbulent energy. Equation of state: ideal gas with adiabatic constant γ=1.4.

There were two variants of computations for the problem above: in one of them two gases of different densities were considered to be various gases, i.e. with different concentrations, and in the second variant both gases were considered to be one and the same material. The "rigid wall" type boundary conditions are specified for all boundaries of the computational domain.

Computations by hydrodynamic code were, generally, the same as those described above. The difference was that for this code specification of pressure was not required in view of the requirement of incompressibility.

2. Results of 3D computations, integral characteristics

Results of computations with two materials are given in Figs.2, 3 in the form of raster patterns of the light substance concentrations at various times and in various horizontal cross-sections.

The flow evolution observed during the first (unstable) phase is similar, in general, to that obtained in the previous computations (see Refs.[2, 5-8]): enlargement of vortexes with time and final tapering-off to a self-similar regime at the end of this phase.

For the given phase, the latter means, in particular, tapering-off to the linear dependence on time for the TMZ width function, L_t (t)

$$F \equiv \frac{1}{t_0}\sqrt{\frac{L_t}{Ag}}\,. \qquad (1)$$

Here, time τ is measured in terms of $t_0 \equiv \sqrt{\frac{L_x}{g}}$, $(\tau \equiv t/t_0)$ and $L_t \equiv (z_2 - z_1)$ is the TMZ width in z direction determined by points z_1, z_2 at which a small enough value ε of perturbation of a hydrodynamic quantity (for example, concentration) is achieved. Assume further that $c_2(z_1)=\varepsilon$, $c_2(z_2)=1-\varepsilon$, c_2 is the mass fraction of the substance having density ρ_2 = n at initial time.

The angle of inclination dF/dτ determines the value of coefficient $\alpha_a = \left(\frac{dF}{d\tau}\right)^2$ in formula for TMZ width during the first (self-similar) phase

$$L_{ta} = \alpha_a A g t^2\,. \qquad (2)$$

Fig. 4 shows plots of F(t) function obtained in computations using formula (1). It follows from Fig.4, that during the first phase F(τ) behavior is almost the same in all variants.

During the second phase, there is an insignificant decrease of F(τ) in one-material computations and then it becomes growing slowly. At the same time, in computations with two materials F(τ) linearly decreases (up to small fluctuations, see below), with its inclination being almost the same in both variants of computations on various grids.

The value of angle of inclination is $\alpha^{(-)} \equiv \frac{dF}{d\tau} \approx -0.084$; the corresponding linear approximation is shown in Fig.4.

Fig.5 shows the time dependence for function

$$F_2 \equiv \frac{1}{t_0}\sqrt{\frac{z_2 - z_c}{Ag}} \tag{3}$$

of z_2 coordinate of the light fluid penetration into the heavy fluid. In general, $F_2(\tau)$ behavior is similar to $F(\tau)$ behavior. As it was expected, TMZ is growing faster towards the light fluid.

During the second phase, hydrostatic equilibrium conditions are violated and waves leading to significant fluctuations of the quantities of interest emerge in the problem, because incompressibility requirement is met with insufficient accuracy (due to the requirement of not too small time step).

Note also that in computations with one material only insignificant decrease of $F_2(\tau)$ is observed during the second phase, then it becomes increasing slowly. At the same time, in two-material computations $F_2(\tau)$ linearly decreases (up to small fluctuations, see below), with its inclination being almost the same in both variants of computations and close to that observed during the experiment. The value of angle of inclination is $\alpha_2^{(-)} \equiv \frac{dF_2}{d\tau} \approx -0.04$; the corresponding approximation is shown in Fig.5.

The value of

$$f \equiv \sqrt{2A\alpha_s} \equiv \frac{d\sqrt{z_2 - z_c}}{d\sqrt{S'}} \tag{4}$$

was measured in papers [9,10]. Here,

$$S' \equiv g_{12}\frac{(t-t_c)^2}{2}, \quad t_c \text{ is the time of maximum } F_2 \text{ value.}$$

Thus, our calculations give us the following value of *f:*

$$f = \frac{dF_2}{d\tau} \cdot \sqrt{A \cdot \frac{2g}{g_{12}}} \approx -0.074 ,$$

which is slightly modulo lower than $f \approx -0.1 \quad (\alpha_s \approx 0.01)$ proposed by the authors of Refs.[9,10] basing on their experiments. Note, however, that the corresponding data of the experiment with S*=360 from [10] shown in Fig.5 give us the value $f \approx -(0.062 \div 0.096) \quad (\alpha_s \approx 0.0038 \div 0.0092)$ that agrees with our computation results. In so doing, we use the values of S(t) stated by the authors of Ref.[10]: g=a_1=6060m/s2, g_{12}=a_2=2450 m/s2.

At the same time, for the experimental data (S*=140, τ*=2.4) [10] the use of the values given in [10] to calculate the values of S(t) (namely, g=a_1=6060m/s2 and g_{12}=a_2=1760 m/s2) leads to the maximum possible value S≈620 which is noticeably lower than S≈790 that follows from the measurements made in [10]. In order to obtain such value of S, one should assume g_{12}=1300 m/s2. The experimental points resultant from data processing are given in Fig.5. It is seen that for the first 6 points the value $f \approx -(0.066 \div 0.071) \quad (\alpha_s \approx 0.0043 \div 0.0051)$ follows after the acceleration sign has changed; this value is lower, on average, than for S*=360 and it is insignificantly lower than our computation result. With regard to the last two points, the value of f appears to be several times lower, however, for these points such small precision of the calculated value of f can be attributed, apparently, to a strong dependence of the found values of τ on the value of g_{12}. It should be emphasized, that the experiment with S*=140 is subject to the effects violating the turbulent flow self-similarity to a higher extent than the experiment with S*=360, because it is more close to the initial stage, where these effects prevail.

Note that for both values S* above, f and, hence, α_s appear to be lower than $f \approx -0.1 \quad (\alpha_s \approx 0.01)$ offered by the authors of Refs. [9,10].

Self-similar regime, for the given problem, also consists in tapering-off to the time-independent value

$$\mathrm{E_m(t) \equiv max(E)} , \tag{5}$$

the maximum (with regard to TMZ width) value of the scaled turbulent energy is

$$E \equiv \frac{k}{L_t g} , \tag{6}$$

where

$$k(z) \equiv E_{ii} , \qquad E_{ik}(z) \equiv \frac{< u_i u_k > - < u_i >< u_k >}{2} , \tag{7}$$

here averaging (denoted by symbol < >) is made over the whole horizontal cross-section z=const. As one can see from Fig.6, the value of E(t) at the end of the first phase reaches the approximately constant value $E = E_a$ in all calculations. With the acceleration sign changed, significant drop of E_m value is observed at first, which is later followed by slow increase of E_m value. During this phase, the both codes (GD *и* HD) give close dependences $E_m(t)$ in computations with one material. In both variants of computations with two concentrations, $E_m(t)$ is going above. Note that in computations with small value of pressure p_0 it goes with large fluctuations.

To give a more valid conclusion concerning self-similar modes, it is required to consider also some other turbulence quantities.

Fig.7 shows the time dependence for the maximum in TMZ value (R_m) of the squared density fluctuation ratio, R:

$$R_m \equiv \max(R); \quad R \equiv \frac{\sigma}{\rho^2}, \tag{8}$$

where $\sigma \equiv < \rho'^2 >$ is the squared density fluctuation value.

One can see from this figure that during the first phase this quantity reaches an approximately constant value in computations with two materials using GD code. With the acceleration sign changed, R_m fluctuations are observed (their value is noticeably higher in computation with small pressure p_0), but, on the average, it remains constant and the same as during the first phase. However, it is possible to note slow (though noticeable) decrease of R_m value depending on time for both computations using GD code.

At the same time, in computations with one material the difference is observed even in the first phase: the value of R_m achieved at the end of the first phase is considerably lower. During the second phase, R_m increase up to very small values is observed, with the R_m (t) behaviors being very close in computations using both GD and HD codes.

Let the maximum in TMZ absolute value of turbulent mass flow for its direction corresponding to unstable conditions be

$$R_{zm} \equiv \max\left(-R_z\right) \tag{9}$$

and the maximum in TMZ absolute value of turbulent mass flow in its direction corresponding to stable conditions be

$$R_{zm-} \equiv \max\left(R_z\right), \tag{10}$$

where $R_z \equiv \frac{r_z}{\sqrt{L_t g}}$, $r_z \equiv < \rho' u_z' >$.

Fig.8 shows the dependence on time of the quantity characterizing the resultant effect of the presence of turbulent mass flows of various signs in TMZ: $\tilde{R}_{zm} = R_{zm-} - R_{zm}$.

As for R_m, it follows from Fig.8 that at the end of the first phase $\tilde{R}_{zm}$ achieves its approximately constant value. One can see that during the second phase the resultant flow, in general, changes its sign with time (up to fluctuations caused by passage of waves) relative to the normal (stable) conditions and this effect becomes noticeable in computations with two materials. In computations with one material, the falling is smoother, an emerging negative flow is smaller; both variants appear to close to each other, except for fluctuations in computation using GD code.

3. Comparison with the results of computations using $k-\varepsilon$ model of turbulence

The problem statement was similar to the previous one, the difference is that small initial values of k and ε were specified.

Fig.9 shows the time dependence of function $F_{2,}$ i.e. of coordinate z_2 of the light fluid penetration into the heavy fluid. It is seen from this figure that at the end of the first phase, with tapering-off to the self-similar mode, the calculated value is $\alpha_{a2} \approx 0.03$ that is close to the results of our previous calculations (see Refs.[7,8]) and the results obtained by the other authors (see Refs.[2,5]). The straight line corresponding to this value is also shown in Fig.9.

During the second phase (after the acceleration sign has changed) one can see a noticeable decrease of the rate of TMZ width growth, however, no reduction of the zone size is observed. Thus, we can conclude that it is impossible to achieve any reduction of the TMZ width using k-ε $k-\varepsilon$ model of turbulence. Unlike the experiment shown in the same figure, the rate of TMZ width growth becomes slightly lower and reaches its constant value at large times. The result agrees with the results of computations from Ref.[11], as well as the results given in Fig.9.

Conclusions

Direct 3D numerical simulation of turbulent mixing for the problem with alternating acceleration sign carried out using gas dynamic (GD) and hydrodynamic (HD) codes of TREK complex showed the following.

In all computations of the first (unstable) phase of mixing, close results concerning changes of TMZ width with time and close maximum in TMZ values of the scaled quantities of turbulent energy, E_m and turbulent flow mass have been obtained, while the maximum in TMZ values of the

squared density fluctuations are noticeably higher in computations with two concentrations, than in computations wit one concentration.

The second phase is implemented after the acceleration sign has been changed. In computations with two materials, linear in time decrease of the TMZ width square root corresponds to this phase that agrees with the known data of experiments (see Refs.[9,10]). Noticeable decrease of the value of turbulent energy E_m is also observed. In this case, maximum in TMZ values of the squared density fluctuation ratio remain unchanged in two-fluid computations, while in one-fluid computations they sharply decrease. The resultant turbulent flow, as a whole, changes it sign (up to fluctuations caused by passage of waves) relative to the normal (stable) conditions, while being significantly lower in its absolute value in one-fluid computations, as compared to two-fluid computations. Accordingly, the TMZ width decrease, after the acceleration sign has changed, is insignificant in one-fluid computations.

In general, it should be noted that the use of one-fluid approach to 3D computations corresponds to mixing fluids, while the multiple-fluid approach correspond to non-mixing fluids.

References

1.K.I. Read. Experimental investigation for turbulent mixing by Rayleigh-Taylor instability // Physica D12, 45, 1984.

2.P.F. Linden, J.M. Redondo, D.L. Youngs. Molecular mixing in Rayleigh-Taylor instability, J.Fluid Mech.1994, Vol.265, P.97-124.

3.G. Dimonte, M. Schneider. Density ratio dependence of Rayleigh-Taylor mixing for sustained and impulsive acceleration histories // Presentation at the 8th International Workshop on the Physics of Compressible Turbulent Mixing. 8th IWPCTM, Pasadena, USA, 2001.

4.Yu.A.Kucherenko, O.E.Shestachenko,Yu.A.Piskunov, E.V.Sviridov, V.M.Medvedev, A.I.Baishev. Experimental investigations of the self-similar regime of different-density gas mixing in the Earth gravity field. // The VI-th Zababakhin Scientific Talks. Collected Abstracts of Presentations, Snezhinsk, 24-28 September 2001.

5.D.L. Youngs. Numerical simulation of mixing by Rayleigh-Taylor and Richtmyer-Meshkov instabilites // Laser and Particle Beams. 1994, Vol. 12, No.4, pp. 725-750.

6.A.A. Stadnik, V.P. Statsenko, Yu.V. Yanilkin, V.A. Zhmailo. Direct numerical simulation of gravitational turbulent mixing. 5rd International Workshop on the Physics of Compressible Turbulent Mixing, Stony Brook ,USA, (1995-20).

7.O.G. Sinkova, A.L. Stadnik, V.P. Statsenko, Yu.V.Yanilkin, V.A. Zhmailo. Three-Dimensional Direct Numerical Simulation of Gravitational Turbulent Mixing // 6rd Inter. Workshop on the Phis. of compr. turbulent mixing. Marseille, France. 1997.P.470-479.

8.Yu.V. Yanilkin, V.P. Statsenko, S.V. Rebrov, O.G. Sin'kova, A.L. Stadnik. Study of gravitational turbulent mixing at large density differences using direct 3D numerical simulation // Presentation at the 8th International Workshop on the Physics of Compressible Turbulent Mixing. 8th IWPCTM, Pasadena, USA, 2001.

9.YU.A. Kucherenko, V.E. Neuvazhaev, A.P. Pylaev. Behaviour of gravitational turbulent mixing region under conditions leading to separation. 4rd International Workshop on The Phisics of compressible turbulent mixing, Cambridge, England, 1993. pp.70-80.

10. Y.A. Kucherenko, S.I. Balabin, R.I. Ardashova, et al. Determination of Space and Time Distributions of the Averaged Density of Substance in the Turbulized Mixture Region at the Stage of Separation. 6th International Workshop on the Physics of Compressible Turbulent Mixing, Marseille, France, 1997, pp.258-265.

11. Z. Zhang and J.Wang, Numerical Simulation of Rayleigh-Taylor instability with the simplified Reynolds Stress Model, // 6rd Inter. Workshop on the Phys. of Compressible Turbulent Mixing, Marseille, France, 1997, pp.569-574.

12. V.A.Andronov, S.M.Bakhrakh, E.E.Meshkov, V.V.Nikiforov, A.V.Pevnitskii, A.I.Tolshmyakov. Experimental investigation and numerical simulation of turbulent mixing in 1D flows. DAN SSSR, V.264, No 1, 1982, pp.76-82.

13. D.L. Youngs, Variable acceleration Rayleigh-Taylor mixing, // 6rd Inter. Workshop on the Phis. of compr. turbulent mixing. Marseille, France. 1997. P.534-538.

14. Yu.V. Yanilkin, V.V. Nikiforov, Yu.A. Bondarenko, E.V. Gubkov, G.V. Zharova, V.P. Statsenko, V.I. Tarasov. Two-parameter model and method for computations of turbulent mixing in 2D compressible flows. 5rd International Workshop on the Physics of Compressible Turbulent Mixing, Stony Brook (USA), 1995.

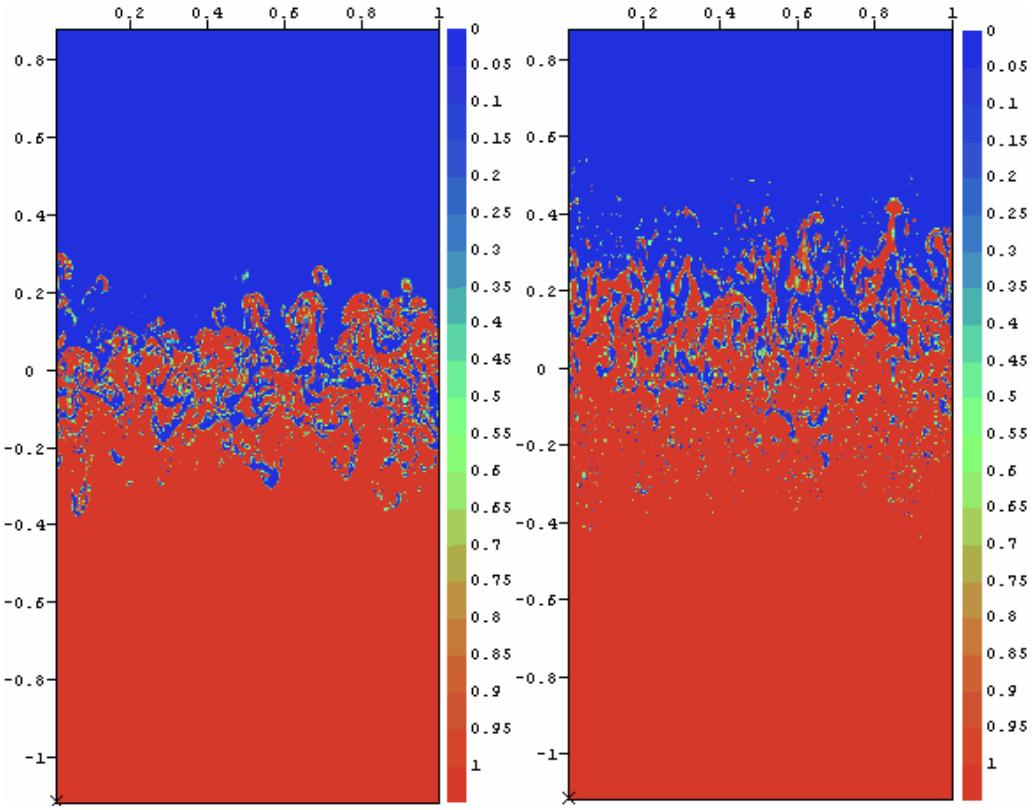

Fig.2. The raster pattern of the light fluid concentration in cross-section y= 0.5, (a) - t=3, (b) - t=5.

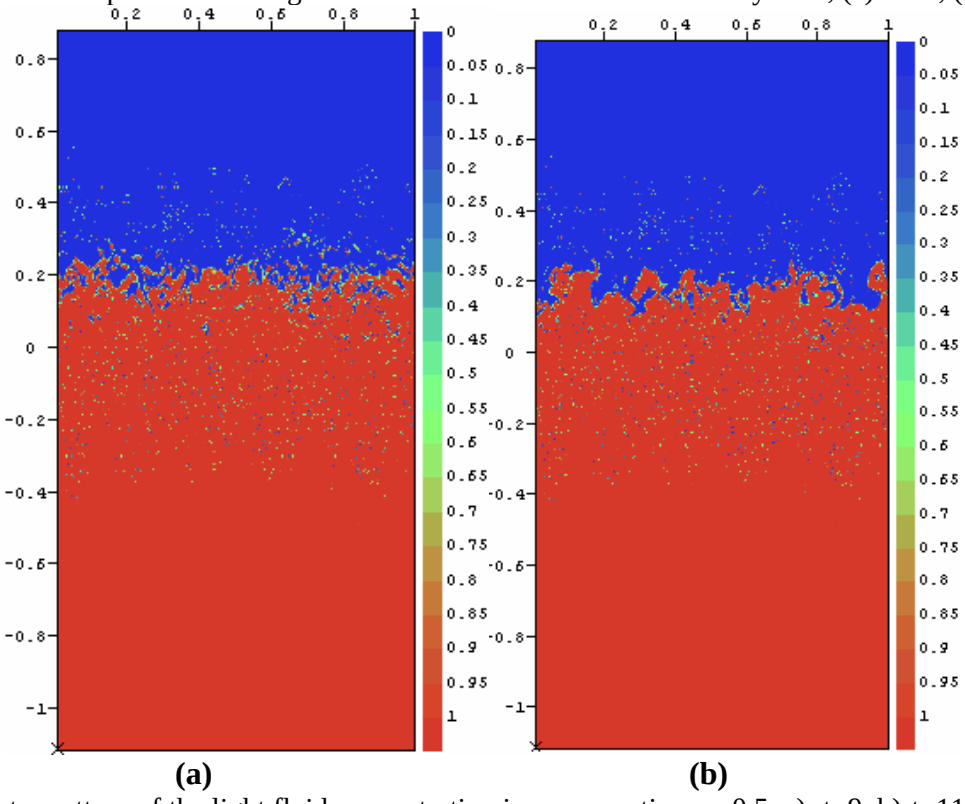

Fig. 3. The raster pattern of the light fluid concentration in cross-section y= 0.5, a) -t=9, b)-t=11.5.

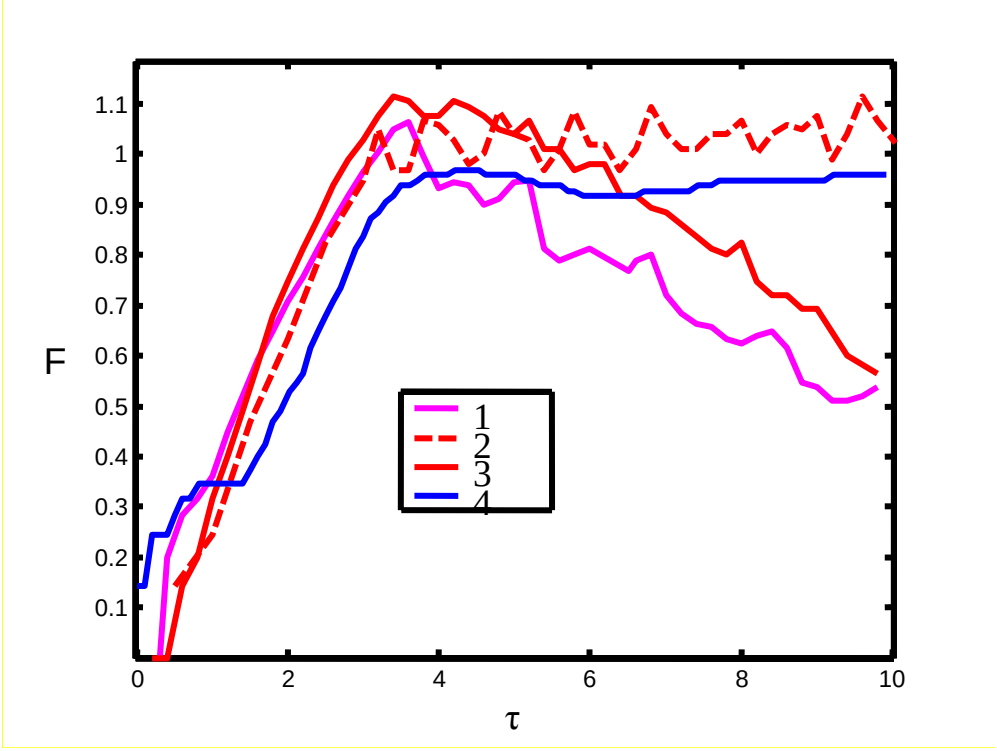

Fig.4.The TMZ width dependence on time: 1 – computations using GD code on grid N_x=200; 2-3 – computations on grid N_x=100; 4 – computations using HD code on grid N_x=100; variants 2 and 4 – computations with one fluid, variants 1 and 3 – computations with two fluids.

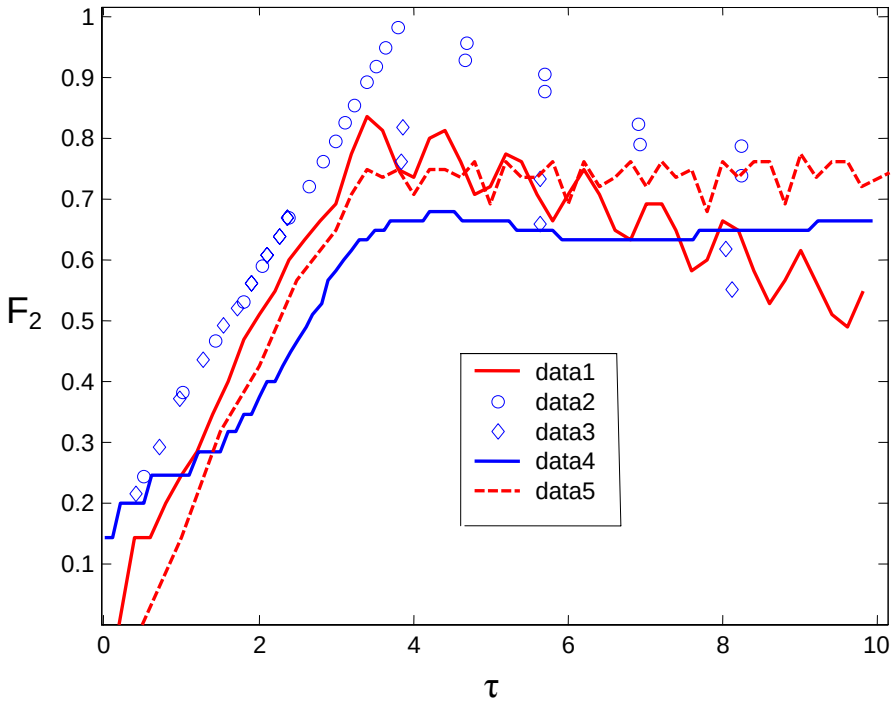

Fig.5.The dependence on time of coordinate z_2 of the light fluid penetration into the heavy fluid: 3D computations on grid N_x=100; 1,5 –computations using GD code; 4 – computations using HD code. Variants 4 and 5 – computations with one fluid, 1 – with two fluids. 2,3 – experiments [10] with S*=360 and S*=140, respectively.

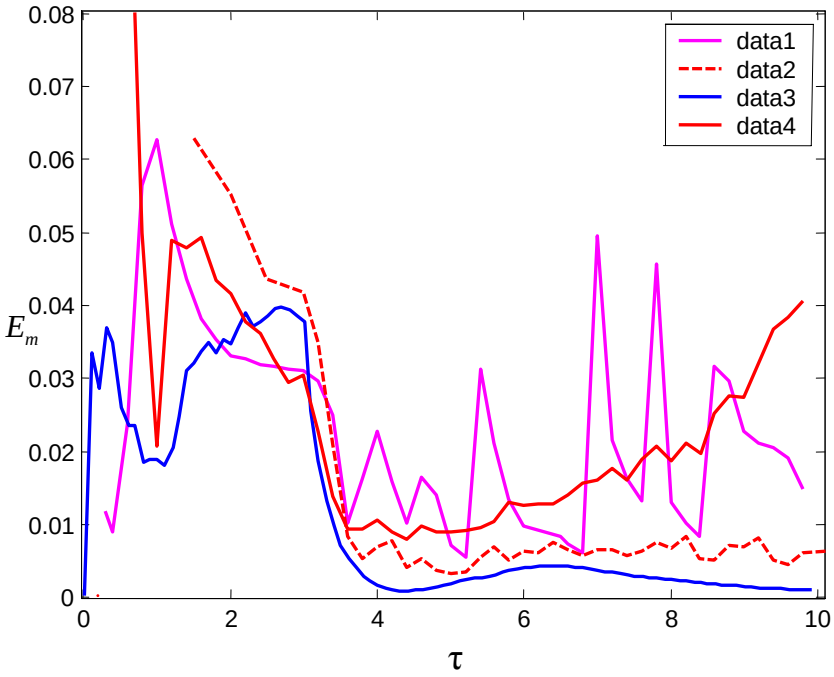

Fig.6. The time dependence of the maximum in TMZ scaled turbulent energy: 1 – computations using GD code on grid N_x=200 with two fluids; 2-4 – on grid N_x=100; 2 ,4 – computations using GD code with one and two fluids, respectively; 3 – computations using HD code with one fluid.

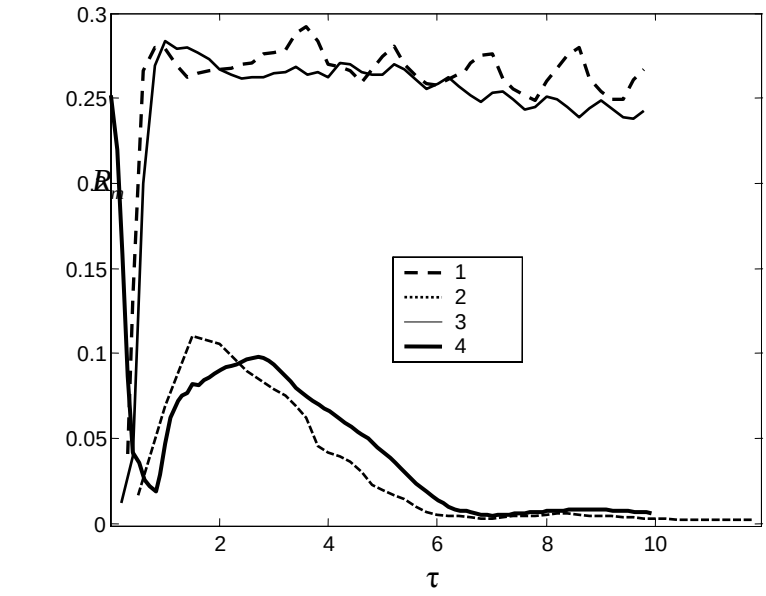

Fig.7. The time dependence of the maximum in TMZ value of squared density fluctuation ratio R_m. Using GD code: 1 – on grid N_x=200, 2,3 – on grid N_x=100. 4 – using HD code on grid N_x=100. Variants 2 and 4 – with one fluid.

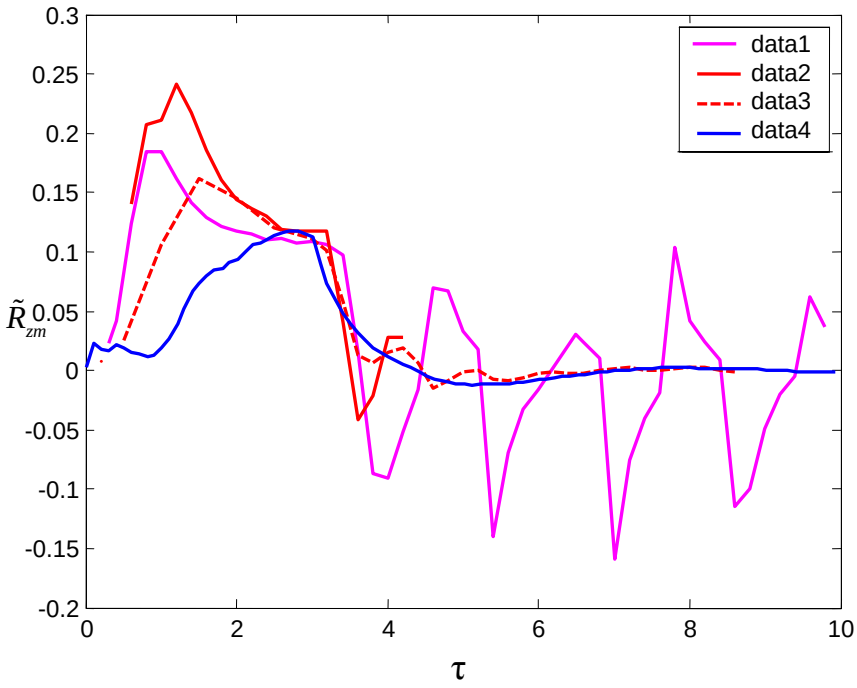

Fig. 8. The dependence on time of the scaled turbulent mass flow $\tilde{R}_{zm}$ in 3D computations using GD code: 1 – on grid N_x =200; 2,3 – on grid N_x =100, 4 – computations using HD code on grid N_x =100. Variants 3 and 4 – with one fluid.

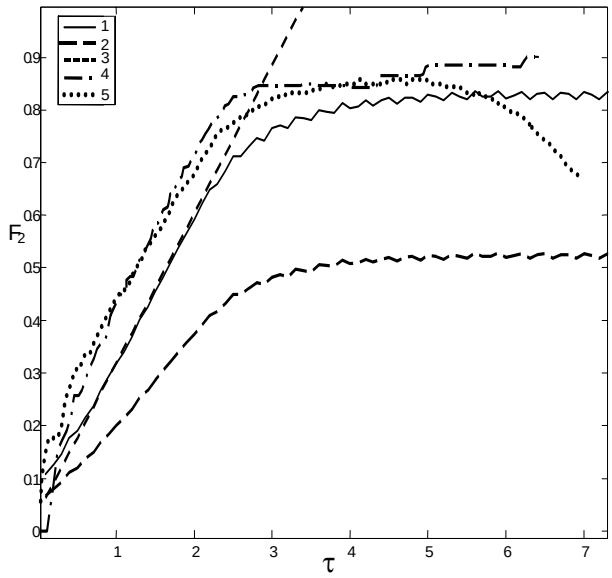

Fig.9.The time dependence of z_2 coordinate of the light fluid penetration into the heavy one. 1, 2 – computations using $k-\varepsilon$ model, 1 – F_2·1.58; 3 – approximation; 4 – computation from [11]; 5 – experimental curve from [9].